Neurotherapeutics (2022) 19:408–420
https://doi.org/10.1007/s13311-021-01176-6

ORIGINAL ARTICLE

IDP-410: a Novel Therapeutic Peptide that Alters N-MYC Stability and Reduces Angiogenesis and Tumor Progression in Glioblastomas

Ricardo Gargini[1] · Berta Segura-Collar[1] · María Garranzo-Asensio[1] · Rafael Hortigüela[1,2] · Patricia Iglesias-Hernández[1] · Daniel Lobato-Alonso[1] · Miguel Moreno-Raja[3] · Santiago Esteban-Martin[3] · Juan M. Sepúlveda-Sánchez[4] · Laura Nevola[3] · Pilar Sánchez-Gómez[1]

Accepted: 14 December 2021 / Published online: 31 January 2022

Abstract

Glioblastomas (GBMs) are the most frequent and highly aggressive brain tumors, being resistant to all cytotoxic and molecularly targeted agents tested so far. There is, therefore, an urgent need to find novel therapeutic approaches and/or alternative targets to bring treatment options to patients. Here, we first show that GBMs express high levels of N-MYC protein, a transcription factor involved in normal brain development. A novel stapled peptide designed to specifically target N-MYC protein monomer, IDP-410, is able to impair the formation of N-MYC/MAX complex and reduce the stability of N-MYC itself. As a result, the viability of GBM cells is compromised. Moreover, the efficacy is found dependent on the levels of expression of N-MYC. Finally, we demonstrate that IDP-410 reduces GBM growth in vivo when administered systemically, both in subcutaneous and intracranial xenografts, reducing the vascularization of the tumors, highlighting a potential relationship between the function of N-MYC and the expression of mesenchymal/angiogenic genes. Overall, our results strengthen the view of N-MYC as a therapeutic target in GBM and strongly suggest that IDP-410 could be further developed to become a first-in-class inhibitor of N-MYC protein, affecting not only tumor cell proliferation and survival, but also the interplay between GBM cells and their microenvironment.

Keywords N-MYC · Peptide inhibitors · Protein stability · Glioblastoma · Glioma · Tumor microenvironment · Angiogenesis

Introduction

Glioblastoma (GBM), classified as a grade 4 isocytrate dehydrogenase 1/2 (IDH 1/2) wild-type astrocytoma, is one of the most aggressive forms of cancer, as well as the most frequent malignant primary tumor of the brain [1]. Surgical removal of the tumor followed by radiotherapy and chemotherapy with temozolomide is the common GBM treatment. However, the invasiveness and proliferation rate of tumor cells, as well as their high resistance to conventional therapies favor the recurrence of GBM, leading to the death of the patients in 15 to 20 months after the first diagnosis [2–4]. The development of new types of drugs, especially those capable of reaching the brain, is necessary to enhance the survival of these patients, who have not seen a therapeutic improvement in the last decades. In this sense, the development of small molecules to inhibit the function of transcription factors (TF), as is the case of inhibitors of Brd4 (Bromodomain containing 4), STAT3 (Signal transducer and activator of

Ricardo Gargini and Berta Segura-Collar contributed equally to this work.

✉ Ricardo Gargini
ricgargini@gmail.com

✉ Laura Nevola
l.nevola@idp-pharma.com

✉ Pilar Sánchez-Gómez
psanchezg@isciii.es

1 Neurooncology Unit, Instituto de Salud Carlos III-UFIEC, Madrid, Spain

2 Centro de Investigaciones, Biológicas Margarita Salas-CSIC, Madrid, Spain

3 IDP Discovery Pharma S.L, Barcelona, Spain

4 Instituto de Investigaciones Biomédicas I+12, Hospital 12 de Octubre, Madrid, Spain

transcription 3), NFκB (nuclear factor kappa-light-chain-enhancer of activated B cells) or MYC, is a major focus of interest in different cancers [5].

The MYC family of oncogenes, which includes *c-MYC*, *L-MYC*, and *N-MYC*, are dysregulated in many neoplasias, associated with poor patients' prognosis [6, 7]. MYC proteins regulate numerous processes such as cell growth, differentiation, and apoptosis, normally through dimerization with MYC-associated protein X (MAX) and formation of a functional transcriptional activator. However, MYC may also bind MYC interacting zinc finger 1, SP1 and other co-factors to repress gene expression [8]. The transcriptional output signature of MYC proteins is highly dependent on the cellular context. L-MYC and N-MYC are distinctly expressed in specific tissues (lung and neuronal tissue, respectively), whereas c-MYC is ubiquitously expressed. *c-MYC* and *N-MYC* can replace each other during normal development [9] or in cancer, where they often show mutually exclusive expression patterns [10, 11].

A two-fold rise in MYC levels suffices to affect cell cycle progression, leading to cancer [12], so the expression of this TF is tightly regulated. Proliferating cells allow for MYC stabilization at a protein level, but quiescent cells degrade the protein through the ubiquitin degradation pathway, a process that depends on the phosphorylation status of MYC proteins [13]. Indeed, overexpression of N-MYC harboring a mutation at threonine 58 that leads to protein stability can originate cerebellar medulloblastomas as well as forebrain gliomas [14]. Direct amplification or overexpression of *MYC* genes have also been found in human brain tumors, including pediatric gliomas, adult GBM, and medulloblastomas [13, 15–19]. Moreover, different oncogenic alterations promote the tumorigenicity of glioma stem cells through c-MYC stabilization [20, 21].

MYC proteins are considered undruggable because they belong to the internally disordered proteins (IDPs) group, which lack a stable 3D structure and exist instead as ensembles of rapidly interchanging conformations [22]. On top of that, their intra-nuclear localization supposes an additional challenge. Still, many efforts have been made over the last years to target MYC genes to treat different cancer types, including inhibiting MYC transcription or transcriptional activity, protein stability, dimerization, immune therapy, and synthetic lethality [23–27]. These have allowed establishing the important role of N-MYC in medulloblastomas and neuroblastomas [13]. However, specific downregulation or inhibition of this gene has not been tested yet in GBMs.

In this work, we confirm the strong expression of N-MYC in human GBM samples and mouse models. Notably, no increase is observed in the amount of *MYCN* mRNA. Moreover, we describe the anti-glioma effect of IDP-410, a stapled peptide specifically designed to target N-MYC. By using primary glioma cell lines, we demonstrate that this novel inhibitor reduces the viability of those cells expressing high levels of this TF. IDP-410 disrupts the N-MYC/MAX complex, reducing the stability of N-MYC protein and the amount of nuclear staining. Systemic treatment with IDP-410 reduces heterotopic and orthotopic glioma growth by attenuating the vascularization of the tumors. Our results show a potential relationship between the function of N-MYC and the expression of mesenchymal/angiogenic genes. Overall, the results presented here suggest that IDP-410 could be a first-in-class inhibitor of N-MYC in GBM, affecting the interplay between the tumor cells and their microenvironment.

Materials and Methods

Human Samples

Normal tissue (NT) was obtained postmortem from non-pathological brain samples. NT and glioma samples (fresh frozen or embedded in paraffin) were obtained after patient's written consent and with the approval of the Ethical Committee at Hospital 12 de Octubre (Madrid, Spain) (CEI 14/023 and CEI 18/024).

Cell Culture

The primary cell lines (Supplementary Table S1) were generated as previously described [28]. They belong to the Biobank of Hospital 12 de Octubre. They were maintained in stem cell medium (Neurobasal (Invitrogen) supplemented with B27 (1:50) (Invitrogen), GlutaMAX (1:100) (Invitrogen), penicillin–streptomycin (1:100) (Lonza), 0.4% heparin (Sigma-Aldrich), and 40-ng/ml EGF, and 20-ng/ml bFGF2 (Peprotech)), and passaged after enzymatic disaggregation using Accumax (Millipore).

GBM6 cells were transduced to stably express the Luciferase reporter. To generate the lentivirus, 293 T cells were transiently co-transfected with 10 µg of pLV-Hygro-luciferase (VectorBuilder), 6 µg of packaging plasmid pCMVdR8.74 (Addgene # Plasmid 22,036), and 4 µg of VSV envelope protein plasmid pMD2G. (Addgene # Plasmid 12,259) using Lipofectamine Plus reagent (Gibco). Lentivirus supernatant was collected and used to infect GBM6 cells, which were selected in the presence of Hygromycin (InvivoGen).

Human brain microvascular endothelial cells (HBMEC) were kindly assigned by Dr. Angel Ayuso-Sacido and were cultured following ATCC recommendations, as previously described [29].

IDP-410 Synthesis and Characterization

The structure and characterization of the chemical scaffold and the analogs of the molecule have been previously described in the patent: Peptides with anti-cancer activity 16/635,902. The linear peptide was synthesized with automatic synthesizer using 9-fluorenylmethoxycarbonyl/tertbutyl solid phase peptide chemistry. Ring-closing metathesis reaction was performed in a solution with a first-generation Grubbs catalyst after cleaving the linear peptide from the resin, as previously described [30]. The compound was purified by HPLC-RP (C-18 column; pump A: H_2O with 0.1% TFA; pump B acetonitrile with 0.1% TFA) using a linear gradient 44–54% of B in 15 min (purity grade 95% by HPLC) and identified by ESI–MS.

In Vitro Treatments

The stock solution of IDP-410 (IDP Discovery pharma) was prepared at 10 mM in PBS. For viability assays, 5000 cells were seeded in triplicate wells of a 96-well microplate coated with matrigel (Bekton-Dickinson, 15 mg/ml stock solution diluted 1:100 in DMEM medium (Lonza)). 24 h later, cells were treated with IDP-410 (at the indicated concentrations in each assay), and viability was measured after 72 h of treatment. For that, cells were incubated with Hoechst 33342 (1:200, Sigma-Aldrich) and propidium iodide (1:1000, Merck), and fluorescence was measured in a Cytell Cell Imaging System (GE Heatlhcare Life Sciences). Wells containing non-treated cells were considered as 100% viability for each tested cell line.

For the N-MYC degradation experiment, GBM6, and GBM7 cells were grown in the presence of DMSO or MG132 (Millipore) 10 µM for 1 h, and then the cells were incubated with IDP-410 (10 µM) for 6 h. Then, the cells were collected and lysed and subsequently analyzed by western blot, as described below.

Wound Healing Assay

HBMEC cells were seeded at a density of 5×10^5 cells per well into 24-well flat-bottom microplates and incubated in 10% FBS-supplemented DMEM until sealed. Then, the wound was performed by scratching across the bottom of the well using a pipette tip. The medium was removed, and the cells were washed with PBS prior to adding the conditioned medium (CM). Glioma CM was obtained by incubating GBM6 cells for 48 h in the presence of 5 µM IDP-410 or PBS. After 48 h, the medium was removed and replaced with a fresh starving medium for 6 h. Then, CM was collected, briefly spun, and the supernatant was used for the wound-healing assays. To calculate the wound-closing rate, pictures were taken at different times, and the wound area was measured as square pixels using ImageJ.

In Vivo Assays

Animal experiments were reviewed and approved by the Research Ethics and Animal Welfare Committee at our institution (Instituto de Salud Carlos III, Madrid) (PROEX 244/14 and 02/16), in agreement with the European Union and national directives. For subcutaneous transplantations, cells (3×10^6) were resuspended 1:1 in culture media and Matrigel (BD) and then subcutaneously injected into athymic nude Foxn1nu mice (Harlan Iberica). When the tumors reached a visible size (300 mm^3 on average), animals started receiving IDP-410 at 15 mg/kg through intravenous (i.v.) injections (twice a week). During the treatment, tumors were measured with a caliper twice a week until mice sacrifice. Tumor volume was calculated as 1/2 ($length \times width^2$). Relative tumor growth was calculated in relation to tumor volume at day 1 of treatment. Control animals were treated with the PBS solvent. Two hours before sacrifice, the animals received intraperitoneal injections of 5-Bromo-2′-deoxyuridine (BrdU) (Sigma Aldrich) (50 mg/kg) in saline solution.

To establish the intracranial tumors, we injected 100,000 GBM6 cells (resuspended in 2 µl of culture stem cell medium) with a Hamilton syringe into the nude mice. The injections were made into the striatum (coordinates: A–P, −0.5 mm; M–L, +2 mm, D–V, −3 mm; related to Bregma) using a Stoelting Stereotaxic device. Two weeks after the tumor implantation, we started treating the animals. For that, IDP-410 was dissolved in PBS + 1% polysorbate and injected subcutaneously (15/mg/kg/day). Control animals were treated with this solvent. Tumor growth was monitored in an IVIS equipment (Perkin Elmer) after intraperitoneal injection of D-luciferin (75 mg/kg; PerkinElmer). Animals were sacrificed when they showed signs of disease, and the brains were processed for cellular and molecular analysis.

Quantitative Reverse-Transcriptase PCR

RNA was extracted from the tissue or the cell pellets using RNA isolation Kit (Roche), and it was digested with DNase I (Roche), according to the manufacturer's instructions. cDNA was synthesized with SuperScript II Reverse Transcriptase (Takara). Quantitative real-time PCR (qRT-PCR) reactions were performed using the Light Cycler 1.5 (Roche) with the SYBR Premix Ex Taq (Takara). The primers used for each reaction are indicated in Supplementary Table S2. Gene expression was quantified by the double delta Ct method.

Immunofluorescent and Immunohistochemical Staining and Quantification

Tumor tissues were embedded in paraffin and cut with a microtome. The slides were heated at 60 °C for 1 h followed by deparaffinization and hydration, washed with water, placed into antigen retrieval solution (pressure-cooking) in 10-mM sodium citrate pH 6.0. Paraffin sections were permeabilized with 1% Triton X-100 (Sigma-Aldrich) in PBS and blocked for 1 h in PBS with 5% BSA (Sigma), 10% FBS (Sigma) and 0.1% Triton X-100 (Sigma). For the detection of ki67 or BrdU, sections were incubated with pre-heated 2 N HCl for 15 min, followed by 10-min incubation with 0.1-M sodium borate pH 8.5, and then continued with the blocking solution, as described above. The following primary antibodies (Supplementary Table S3) were incubated O/N at 4 °C. The second day, sections were washed with PBS three times prior to incubation with the appropriate secondary antibody (Supplementary Table S3) for 2 h at room temperature. Prior to coverslip application, nuclei were counterstained with DAPI. Imaging was done with a Leica SP-5 confocal microscope. Otherwise, IHC sections were incubated with biotinylated secondary antibodies (1:200 dilution). Target proteins were detected with the ABC Kit and the DAB kit (Vector Laboratories).

For quantification, slides were scanned at 63 × or 40 × magnification. The number of BrdU-positive cells per field was counted with Fiji-ImageJ software and normalized with the total number of cells. For the quantification of the vasculature, we counted the number of dilated vessels per field, subtracted from endomucin IHC.

Western Blot Analysis

Protein extracts were prepared by re-suspending cell pellets or tumor tissue samples in a lysis buffer (50-mM Tris (pH 7.5), 300-mM NaCl, 0.5% SDS, and 1% Triton X-100) and incubating the cells for 15 min at 100 °C. The lysed extracts were centrifuged at 13,000 g for 10 min at room temperature, and the protein concentration was determined using a commercially available colorimetric assay (BCA Protein Assay Kit). Approximately 30 µg of protein was resolved by 10% or 12% SDS-PAGE, and they were then transferred to a nitrocellulose membrane (Hybond-ECL, Amersham Biosciences). The membranes were blocked for 1 h at room temperature in TBS-T (10-mM Tris–HCl (pH 7.5), 100-mM NaCl, and 0.1% Tween-20) with 5% skimmed milk, and then incubated overnight at 4 °C with the corresponding primary antibody (Supplementary Table S3) diluted in TBS-T. After washing 3 times with TBS-T, the membranes were incubated for 2 h at room temperature with their corresponding secondary antibody (Supplementary Table S3) diluted in TBS-T. The proteins were visible by enhanced chemiluminiscence with ECL (Pierce) using Amersham imager 680, and the signal was quantified by Fiji-ImageJ software.

Immunoprecipitation

GBM6 cells were incubated in the presence of DMSO or IDP-410 (5 µM) for 6 h. Then, the cells were collected, washed in PBS, and the protein extracts were generated in ice-cold lysis buffer (50-mM Tris–HCl [pH 7.6], 150-mM NaCl, 1% Triton X100, 0.5% sodium deoxycholate, 1-mM phenylmethylsulfonyl fluoride, 1-µg/ml leupeptin) during 30 min. After that, the extracts were pre-cleared for 1 h with Protein A/G-Sepharose (Santa Cruz Biotechnology, Inc.) and immunoprecipitated (IP) using anti-N-MYC antibodies (Cell signaling) or IgG as a control. The IP fractions were analyzed by WB with N-MYC (Santa Cruz Biotech) and MAX (Cell signaling) antibodies.

In Silico Analysis

The Cancer Genome Atlas (TCGA) GBM dataset was accessed via UCSC xena-browser (https://xenabrowser.net) for extraction of N-MYC gene's expression level.

Statistical Analysis

GraphPad Prism 5 software was used for data presentation and statistical analysis. For bar graphs, the level of significance was determined by a two-tailed un-paired Student's *t*-test. The difference between experimental groups was assessed by Paired *t*-test and one-way ANOVA. To analyze the survival of nude mice, we used the Kaplan–Meier method and evaluated with a two-sided log-rank test. For correlation analysis between each gene, expression data were tested by Pearson's correlation coefficient and Spearman's correlation coefficient. *P* values < 0.05 were considered significant (*$p < 0.05$; **$p < 0.01$; *** $p < 0.001$; **** $p < 0.0001$; n.s., non-significant). All quantitative data presented are the mean ± SEM.

Results

N-MYC is Highly Expressed in Gliomas

To evaluate whether N-MYC is dysregulated in GBM, we first studied its presence by quantifying its RNA levels. We did not find an increase in *N-MYC* transcription in GBM samples compared to normal brain, both in our cohort (Fig. 1a) or in the analysis of TCGA samples (RNAseq or microarray data) (Supplementary Fig. 1a, b). By contrast, using protein extracts from patients' samples we observed a clear upregulation of N-MYC protein in GBMs compared to non-tumor (NT) tissues (Fig. 1b, c). Notably, compared to N-MYC-low

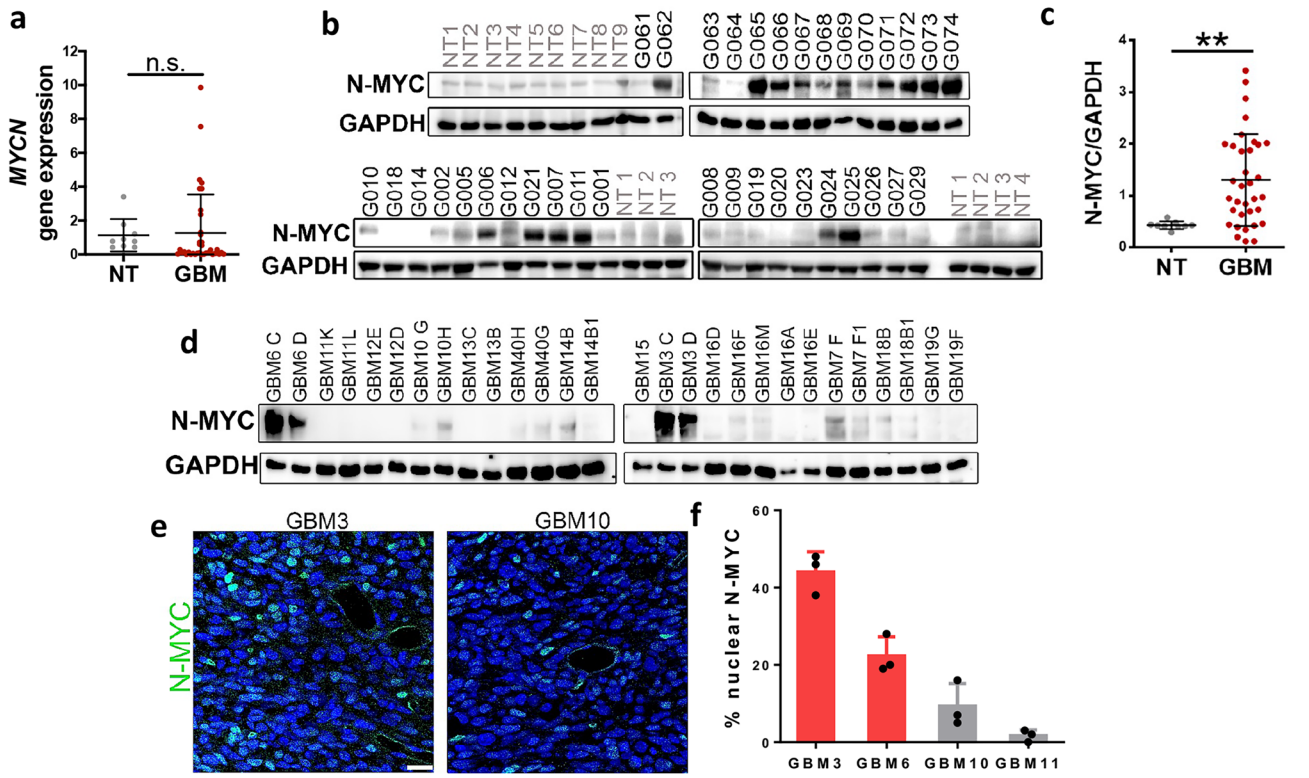

Fig. 1 N-MYC expression in gliomas. **a** Quantification of *N-MYC* mRNA levels by quantitative reverse-transcriptase PCR (qRT-PCR) in a cohort of human glioblastomas (GBM) and normal brain tissues (NT) ($n=35$ and $n=9$). *HPRT* was used for normalization. **b–c** Western blot (WB) analysis of N-MYC levels in the cohort of GBM ($n=35$) and NT ($n=9$) and quantification in **c**. GAPDH was used as a loading control. **d** WB analysis of N-MYC levels in tumor tissue from a panel of PDXs (patient-derived xenografts). Alphabet letters next to the numbers refer to different tumors generated from the same cell line. GAPDH was used as a loading control. **e** Representative images of the immunofluorescence staining of N-MYC in the PDX's tumor tissue. **f** Quantification of cells with nuclear N-MYC in (e). $^{**}p<0.01$; n.s., non-significant

GBMs, tumors with high expression of N-MYC protein display a much more florid and aberrant vasculature (Supplementary Fig. 1c), which is a hallmark of tumor aggressiveness [31].

We also used a cohort of patient-derived xenografts (PDX), and we noticed that some of them also express high levels of N-MYC protein (Fig. 1d), with frequent nuclear staining in the mouse tumors (Fig. 1e) and a strong consistency between the WB and the IF quantification (Fig. 1f). These results confirm the increased levels of N-MYC protein in GBM and suggest that the main mechanisms for this upregulation must be related to increased translation and/or stabilization of the protein. Moreover, they suggest that increased N-MYC expression could be associated with the progression of the glioma disease.

Effect of IDP-410 N-MYC Inhibition in Glioma Growth In Vitro

We studied IDP-410, a novel stapled peptide designed to specifically target and inhibit the function of N-MYC, as therapeutic agent in GBM, its mechanism of action, and the biological consequences of inhibiting N-MYC in vitro. For that, we first analyzed the levels of expression of N-MYC in a battery of primary GBM cell lines (Fig. 2a). The exposure of GBM6 (high N-MYC expression) to increasing concentrations of IDP-410 clearly reduced the viability of the cells (Fig. 2b). Moreover, 10 µM of IDP-410 triggered the cell death of all the primary cell lines expressing high levels of N-MYC (Fig. 2c). By contrast, there was very little effect of this compound in GBM8, GBM10 or fibroblasts, which express reduced amounts of N-MYC (Fig. 2a and Supplementary Fig. 1d). A direct comparison of the effect of IDP-410 in GBM6 (high N-MYC), GBM2 (low N-MYC), and fibroblasts (no N-MYC) (Fig. 2d) showed the strong correlation between the expression of the target and the sensitivity to the drug (Fig. 2e), reinforcing its specificity.

IDP-410 Induces N-MYC Protein Degradation In Vitro and Disrupts N-MYC/MAX Complex

The incubation of GBM6 cells with increasing amounts of IDP-410 for 6 h reduced the amount of N-MYC protein in

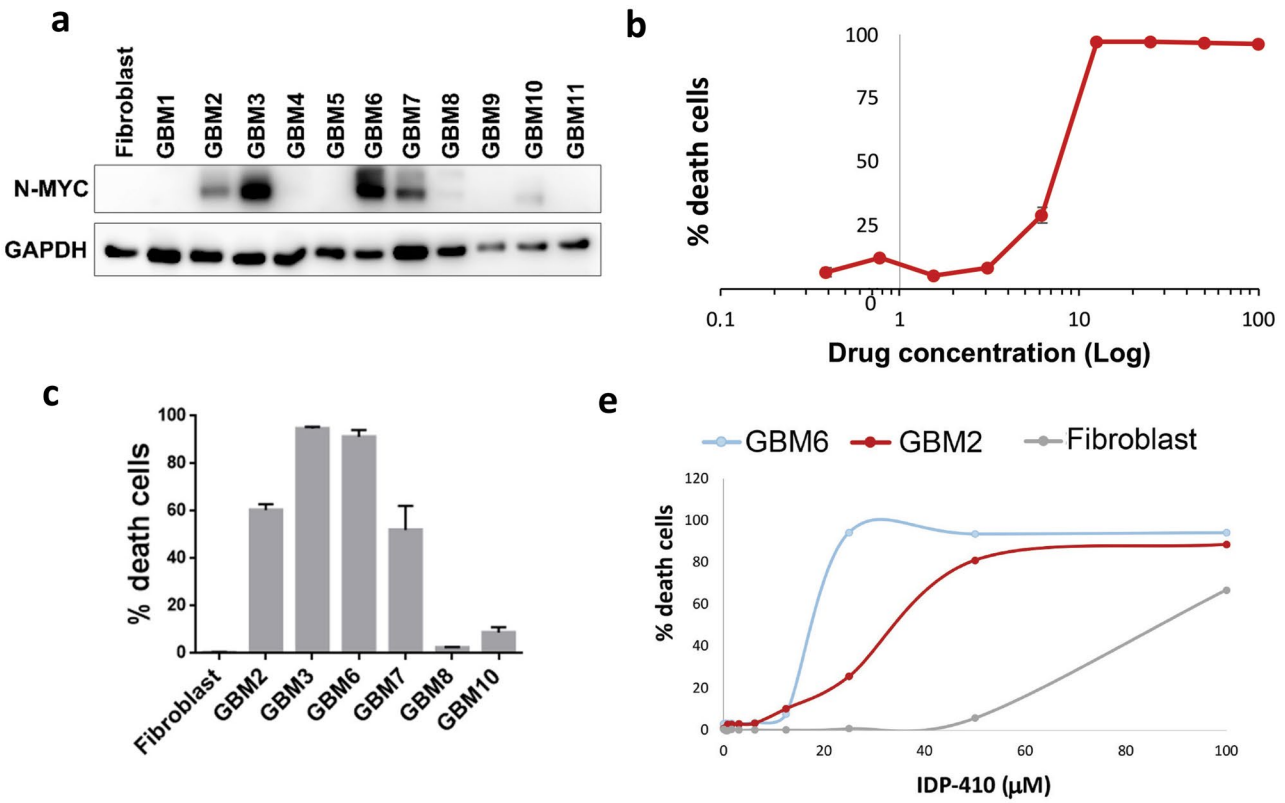

Fig. 2 IDP-410 inhibits gliomas growth in vitro. **a** Western blot (WB) analysis of the levels of N-MYC in a panel of human GBM cells. Diploid human fibroblasts were used as a non-tumor control. GAPDH was used as a loading control. **b** Determination of the percentage of cell death in GBM6 cells exposed to increasing concentrations of IDP-410. **c** Analysis of the percentage of dead cells after IDP-410 treatment of a panel of human GBM cells. **d** Analysis of cell death in the presence of increasing concentrations of IDP-410 in cells with high (GBM6), low (GBM2), or no (fibroblasts) N-MYC expression

the cells (Fig. 3a, b). Notably, the enhanced degradation induced by IDP-410 was blocked in the presence of the proteasome inhibitor MG132, both in GBM6 and GBM7 cells (Fig. 3c–e). We also observed an impairment of N-MYC and MAX interaction in the presence of IDP-410 (Fig. 3f). Taking together, these results suggest that the IDP-410 inhibitory effect is associated with the dissociation of the N-MYC/MAX complex and the degradation of N-MYC.

IDP-410 Suppresses Glioma Growth In Vivo

To evaluate whether the effect of IDP-410 observed in vitro translates to an in vivo setting, we injected GBM6 cells subcutaneously in immunodeficient mice and treated the animals intravenously (i.v.) with IDP-410. The growth curve of the tumors shows that systemic treatment with IDP-410 reduced significantly the tumor size, in comparison to vehicle (PBS) (Fig. 4a, b). Immunofluorescence staining of tissues from both sets of mice demonstrated a reduced nuclear N-MYC expression after IDP-410 treatment (Fig. 4c). Furthermore, BrdU incorporation was reduced in IDP-410 treated mice in comparison with control tumors (Fig. 4d, e), whereas the percentage of apoptotic cells (measured through activated caspase 3 staining) was not different between the two groups of mice (Supplementary Fig. 2). These results suggest that N-MYC inhibition impairs the growth of GBM tumors but does not promote cell death in immune-suppressed, tumor-bearing mice xenografts.

To determine if IDP-410 is able to cross the blood brain barrier and block the growth of orthotopic gliomas, we injected GBM6 cells into the brain of nude mice. Two weeks later, we started treating the animals with vehicle (polysorbate 1% in PBS) or IDP-410, injected subcutaneously. To allow daily treatment with IDP-410, we switch to the subcutaneous route of administration. No local or systemic adverse effects were detected during the whole treatment (5 × week, during 4 weeks). As the cells express the luciferase reporter, we were able to follow up tumor progression in situ, and we determined that IDP-410 reduced the growth of GBM6 cells (Fig. 5a). Moreover, it increases the survival or the tumor-bearing animals (Fig. 5b). The analysis of the excised tumors showed a strong downregulation of nuclear N-MYC in IDP-410-treated samples (Fig. 5c) and a decrease in the amount of N-MYC protein, measured by WB

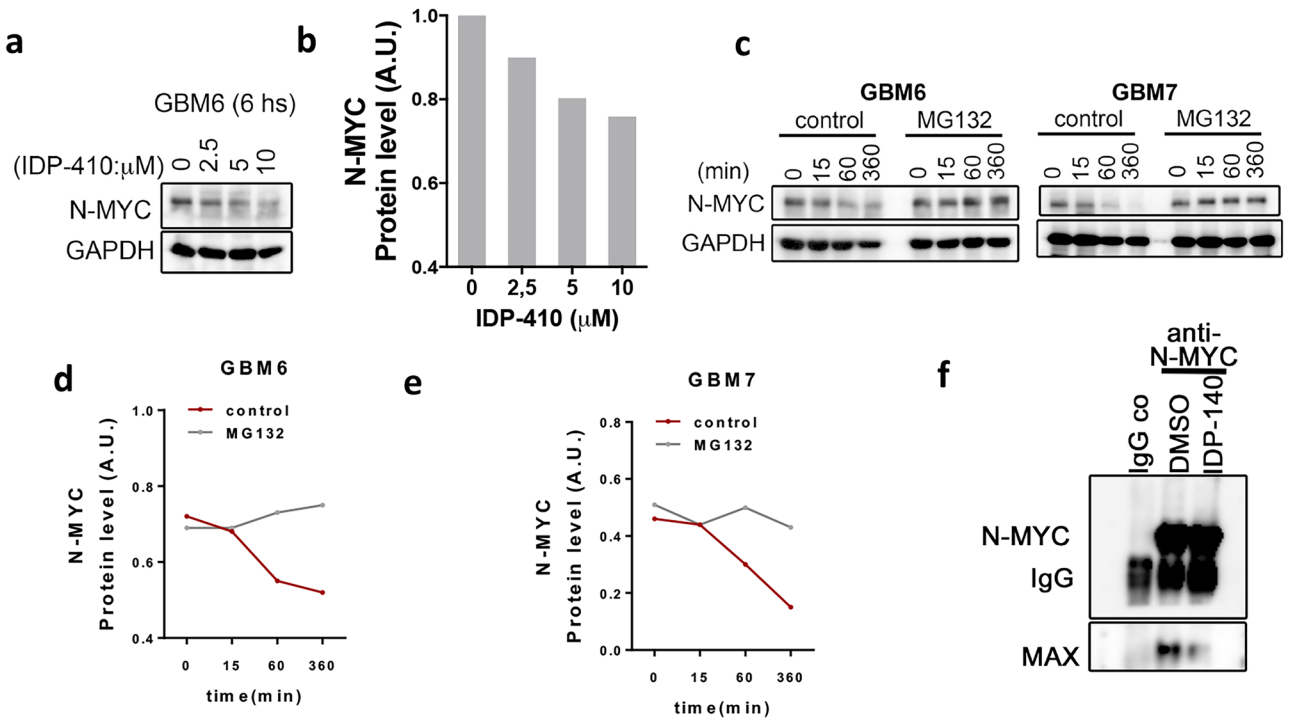

Fig. 3 IDP-410 induces N-MYC degradation. **a–b** Western blot (WB) (**a**) and quantification (**b**) of N-MYC levels in GBM6 cells treated for 6 h with increasing IDP-410 concentrations. GAPDH was used as a loading control. **c** WB analysis of N-MYC expression in GBM6 and GBM7 cells, incubated for different times in the presence of IDP-410 (10 μM), with or without the proteasome inhibitor MG132 (10 μM). GAPDH was used as a loading control. **d–e** Quantification of the WB in (**c**) for GBM6 (**d**) and GBM7 (**e**) cells. **f** Extracts from GBM6 cells, incubated in the presence of DMSO or IDP-410, were immunoprecipitated (IP) using an excess of anti-N-MYC antibodies. The IP fractions were analyzed by WB with N-MYC and MAX antibodies. Control IP with IgG is shown on the left lane

(Fig. 5d). Given the similarities in structure and function among the MYC family members, we wondered if IDP-410 could have an effect also on C-MYC stability. In that sense, no change in the levels of C-MYC protein was observed in the IDP-410-treated tumors (Fig. 5d), suggesting a high specificity of the compound. In agreement with the results obtained in the heterotopic tumor setting, the amount of proliferative cells in the intracranial tumors was also diminished after systemic IDP-410 treatment (Fig. 5e). Altogether, these results suggest that the IDP-410 reaches the brain, decreases the stability of N-MYC protein, and inhibits the growth of GBM cells.

IDP-410 Affects Tumor Proliferation and Vascularization in Treated Mice

MYC proteins regulate the crosstalk between the tumor and the host and have been linked to processes of proliferation and angiogenesis [32–34]. To explore the possible anti-tumor mechanisms of N-MYC inhibition by IDP-410, we selected a series of 27 genes known to be regulated by N-MYC and mainly associated with these two processes (Fig. 6a). We analyzed the expression of all these genes, and we observed that the mRNA expression of some of them was reduced when GBM6 and GBM3 cells were cultured in the presence of IDP-410 (Fig. 6b, c). Notably, a very similar inhibition pattern was observed in human tumors with low levels of N-MYC protein compared to N-MYC high tumors (Fig. 6d) or in the intracranial GBM6 xenografts after systemic IDP-410 treatment (Fig. 6e). Furthermore, we confirmed that the expression of important angiogenesis- (*VEGFA*, VEGF) and proliferation- (*MIK67*, Ki67) related genes correlated positively with N-MYC protein levels in a panel of glioma PDXs (Fig. 6f, g; Supplementary Fig. 3). These results could be related with the differences observed in the vascular phenotype of N-MYC-high and N-MYC-low tumors (Supplementary Fig. 1c).

It is well known that glioma cells, particularly in high-grade tumors, express a variety of genes that promote different steps of the angiogenesis process [31]. To study if N-MYC inhibition by IDP-410 could affect this pro-angiogenic function of gliomas, we first performed an in vitro assay using GBM6 cells. We examined the effect of conditioned media (CM) from these glioma cells (treated or not with IDP-410) on the wound healing capacity of HBMEC cells. Figure 7a, b show that treatment with IDP-410 impaired the effect of glioma CM on the endothelial migration of HBMEC cells.

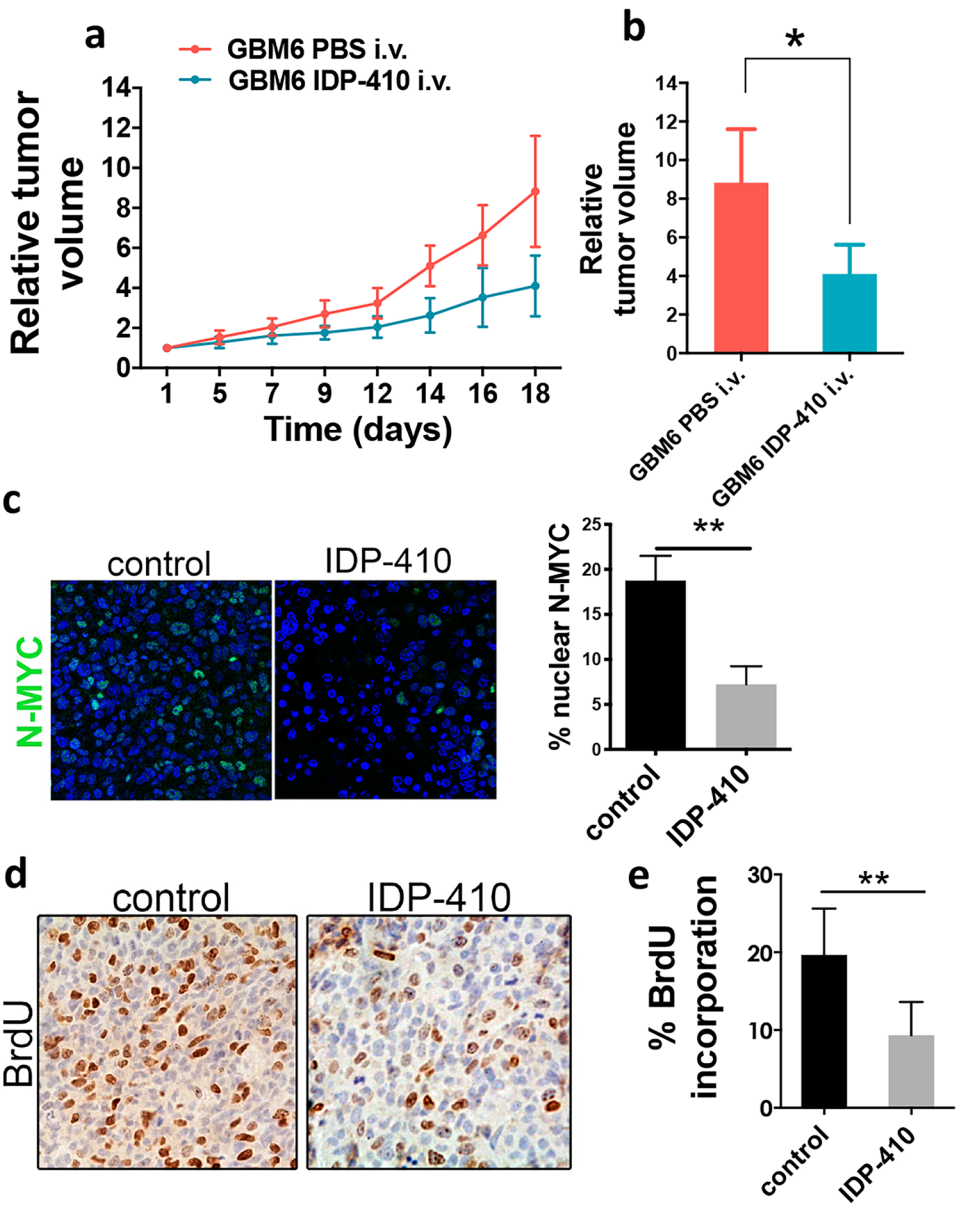

Fig. 4 Systemic IDP-410 impairs the subcutaneous growth of gliomas. **a** Growth curve of GBM6 cells implanted in the flank of nude mice, which were treated by bolus intravenous route (i.v.) with vehicle or IDP-410 twice a week (dose 15 mg/kg). **b** Relative tumor volume at the final end point in (a). **c** Representative images of the immunofluorescence analysis of nuclear N-MYC in tumors treated with vehicle (control) or IDP-410. Quantification is shown on the right (n = 3 / condition). **d**–**e** Determination of tumor cell proliferation measured by incorporation of BrdU and quantified using immunohistochemistry in tumors treated with vehicle (control) or IDP-410 (n = 3 / condition). $*p < 0.05$; $**p < 0.01$

We have recently shown that mesenchymal transformation is key to induce angiogenesis in GBM, even for the generation of tumor blood vessels [29]. When we characterized the tumor tissue from IDP-410-treated animals, we observed a clear reduction on the amount of TAZ and αSMA in comparison with control samples (Fig. 7c). These two proteins are well-known mesenchymal factors [35], which are associated with the neovascularization processes in gliomas [29]. Apart from that, we observed that IDP-410-treated tumors contained reduced levels of the angiogenic factor VEGF (Fig. 7d). In addition, the IHC staining with endomucin antibodies showed a strong reduction in the number of dilated blood vessels in the presence of IDP-410 (Fig. 7e). Taken together, our results suggest that the anti-tumor effect of N-MYC inhibition by IDP-410 is mediated, at least in part, by the decrease in tumor-cell proliferation and by the reduction of neo-vascularization processes.

Discussion

GBM is one of the deadliest tumor types with a very short life expectancy upon diagnosis. Its treatment does not succeed mainly because of its highly heterogeneous and plastic nature [37]. Thus, there is an urgent need to search for new therapeutic strategies. MYC proteins are one of the most wanted targets due to their notorious oncogenic features [5, 6, 23, 26]. However, a long standing consideration for the clinical development of MYC inhibitors is the potential side effects due to its capacity to regulate proliferation in

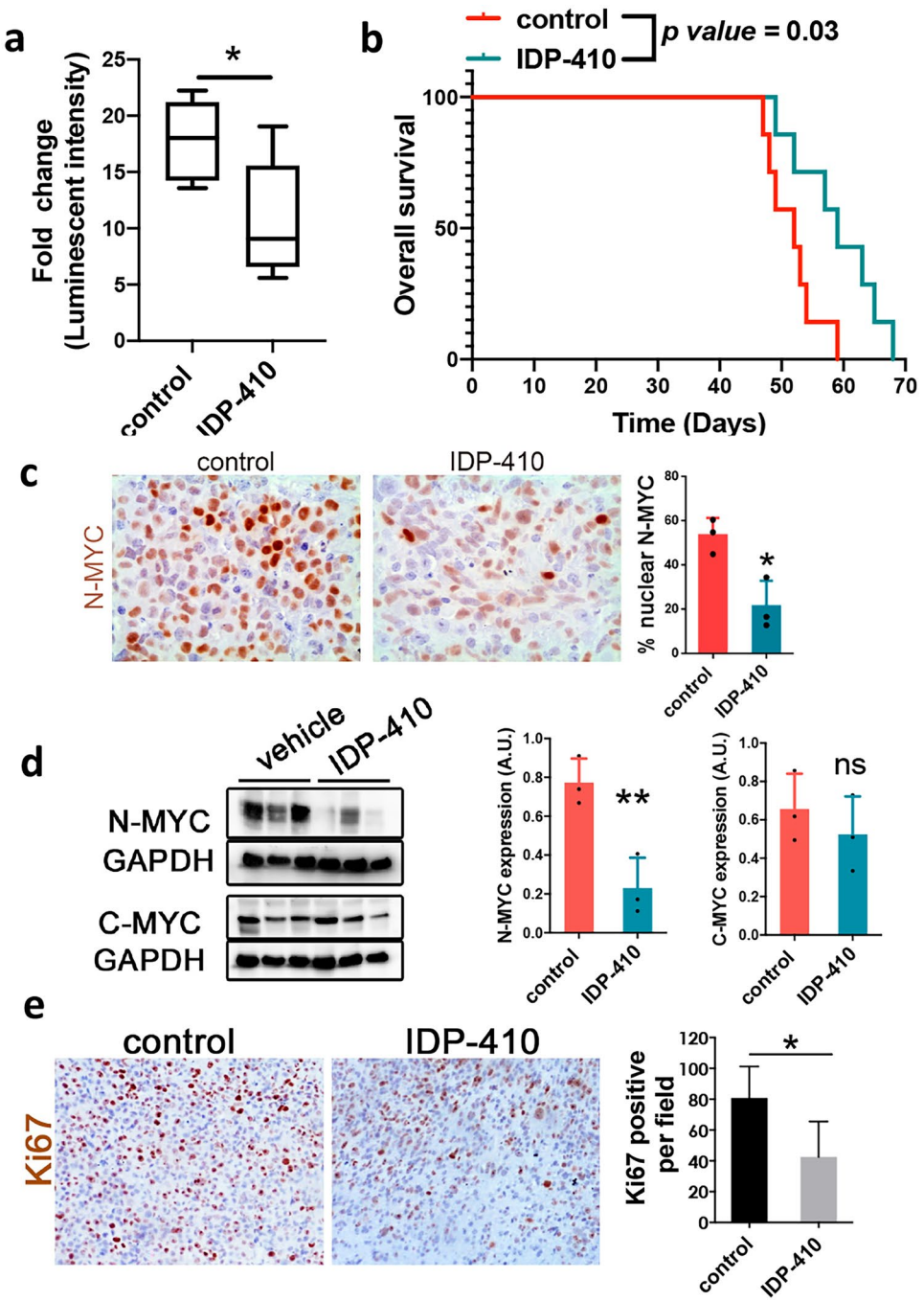

Fig. 5 Systemic IDP-410 impairs the intracranial growth of gliomas. **a** GBM6 cells were intracranially injected in nude mice, and the animals were treated with vehicle (control) or IDP-410 (15 mg/kg; 5 days a week). The graph shows the fold increase in luminescence (between days 40 and 52 after cell injection) in control and IPD-410 treated mice. **b** Kaplan–Meier survival curve of GBM6-bearing mice treated with vehicle (control) or IDP-410. **c** Representative pictures of the immunohistochemical (IHC) staining of N-MYC in tumors from (**b**). Quantification of the nuclear N-MYC staining is shown on the right ($n=3$ / condition). **d** Western blot analysis of N-MYC and C-MYC levels in GBM6 intracranial tumors from (**b**). GAPDH was used as a loading control. Quantification is shown on the right ($n=3$ / condition). **e** Representative pictures of IHC staining of Ki67 in tumors from (**b**). Quantification is shown on the right ($n=3$ / condition). $^{*}p<0.05$, $^{**}p<0.01$

normal tissues. Indeed, systemic inhibition of Myc in transgenic mice models for continuous long periods (4 weeks) was shown to affect high proliferating tissues, such as skin and gastrointestinal tract, but found to be well tolerated, not to alter the homeostasis of the tissues, and the effect readily reversed when Myc was reactivated [38]. In that sense, targeting specifically N-MYC, with a more neural-restricted pattern of expression, has become of interest for many pediatric cancers but also for certain adult neoplasia, including GBM [24].

Here, we have confirmed the overexpression of *N-MYC* gene compared to normal tissue in a percentage of human GBM samples and PDXs. Interestingly, we found no correlation between the levels of protein and mRNA. This suggests that protein stabilization is an important regulatory event and that *N-MYC* transcriptional data cannot be used to evaluate the overexpression of N-MYC protein in gliomas [19]. More importantly, we show here compelling evidence supporting the anti-tumor effect of a novel stapled peptide IDP-410 specifically designed to target

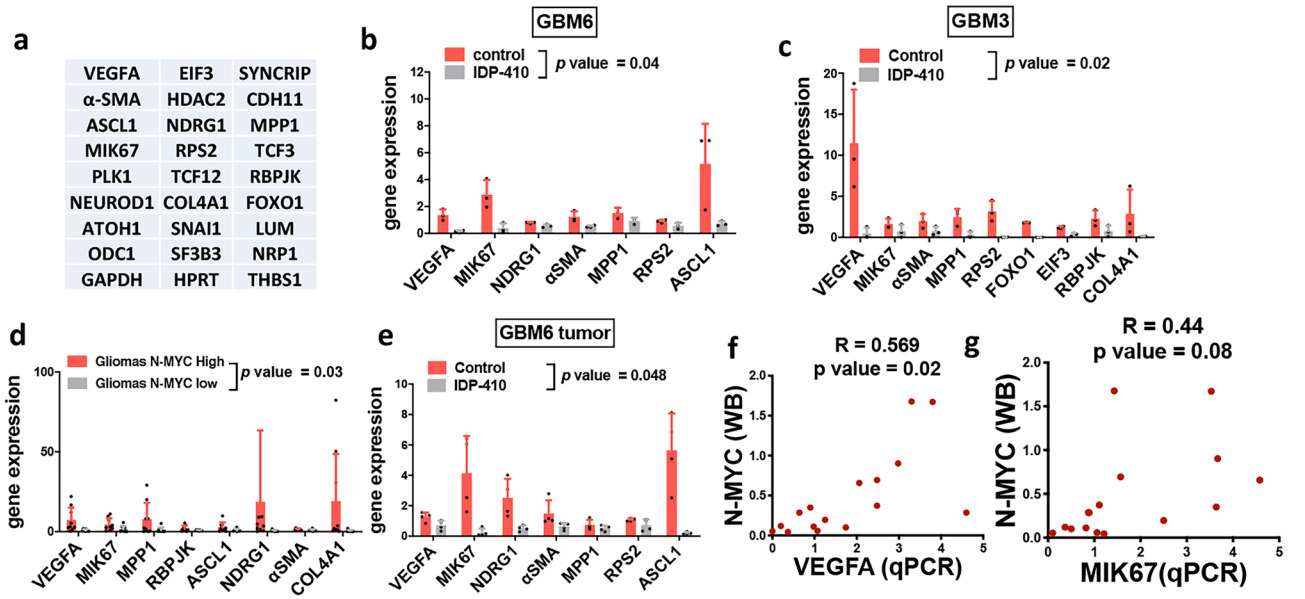

Fig. 6 Effect of IDP-410 in proliferation and angiogenesis-related genes regulated by N-MYC in gliomas. **a** N-MYC upregulated gene signature. **b–c** Quantitative reverse-transcriptase PCR (qRT-PCR) analysis of several N-MYC-related genes (from **a**) in GBM6 (**b**) and GBM3 (**c**) cells treated with vehicle (control) or IDP-410. *HPRT* was used for normalization. **d** qRT-PCR analysis of a signature of N-MYC-related genes in GBM tumors with high- and low-N-MYC protein levels. **e** qRT-PCR analysis of a signature of N-MYC-related genes in GBM6 intracranial tumors from Fig. 5. **f–g** Pearson's correlation analysis between the expression of *VEGFA* (**d**) and *MKI67* (**e**), and the amount of N-MYC protein in a panel of PDXs (Supplementary Fig. 3)

N-MYC in those GBM expressing high levels of N-MYC, both in vitro and in vivo. These results demonstrate the therapeutic potential of IDP-410, which shows capacity to reach subcutaneous and intracranial tumors when administered systemically, with high tolerability. Moreover, the data suggest that N-MYC (protein, not mRNA) should be used as a biomarker.

The nuclear localization of MYC proteins and their intrinsically disordered structure hampers the development of classical small molecule inhibitors against these TFs. Strategies to impair MYC protein function via its transcription and protein or mRNA stability have been developed and some of them have reached the clinic [5, 23, 26, 27]. The most recent example is Omomyc, a miniprotein analog to cMYC currently in phase I for treatment of solid tumors (NCT04808362). It was shown that Omomyc, when conditionally expressed in transgenic models, antagonizes the function of MYC family members and reduce the growth of different types of cancer including GBMs [26]. When administered systemically and intranasally, Omomyc was shown to inhibit tumor growth in lung cancer animal models [39]. However, its potential to reach the brain and act against gliomas has not been evaluated [40].

Our results show that the IDP-410 peptide acts by reducing the interaction of N-MYC with its partner MAX and favoring the degradation of the protein. Systemic IDP-410 treatment induced a decrease in cell proliferation and a clear inhibition of glioma vascularization. In agreement with that, IDP-410 reduced the pro-angiogenic properties of glioma cells in vitro. As a possible mechanism to explain this effect, we observed a strong downregulation of *VEGFA* expression in tumors treated with IDP-410. Moreover, we show a significant correlation between *VEGFA* transcription and the amount of N-MYC protein in GBM xenografts. VEGFA, which is normally secreted by tumor cells, is a key player in angiogenesis as it binds to the endothelial VEGFR2 and promotes proliferation and migration, leading to new vessel-like structures [41–43]. Therefore, our results suggest for the first time a direct regulation of GBM angiogenesis by N-MYC inhibition through the modulation of the expression of *VEGFA* and possibly other vascular-related molecules. This is in agreement with the widely accepted role of c-MYC as a modulator of different aspects of the tumor microenvironment, including the vasculature [32, 44] and with the correlation of *N-MYC* amplification with angiogenesis in neuroblastoma [45].

High-grade gliomas are extremely dependent on their vascular microenvironment, which allows the tumor to gather needed nutrients and oxygen for its growth and promotes the progression of the disease. Florid angiogenesis is associated with the appearance of mesenchymal features, which is linked to the aggressiveness of gliomas [29]. Furthermore, tumor cells that have become mesenchymal invade the adjacent parenchyma or may even interact with endothelial cells, a property that allows them to govern the brain vasculature

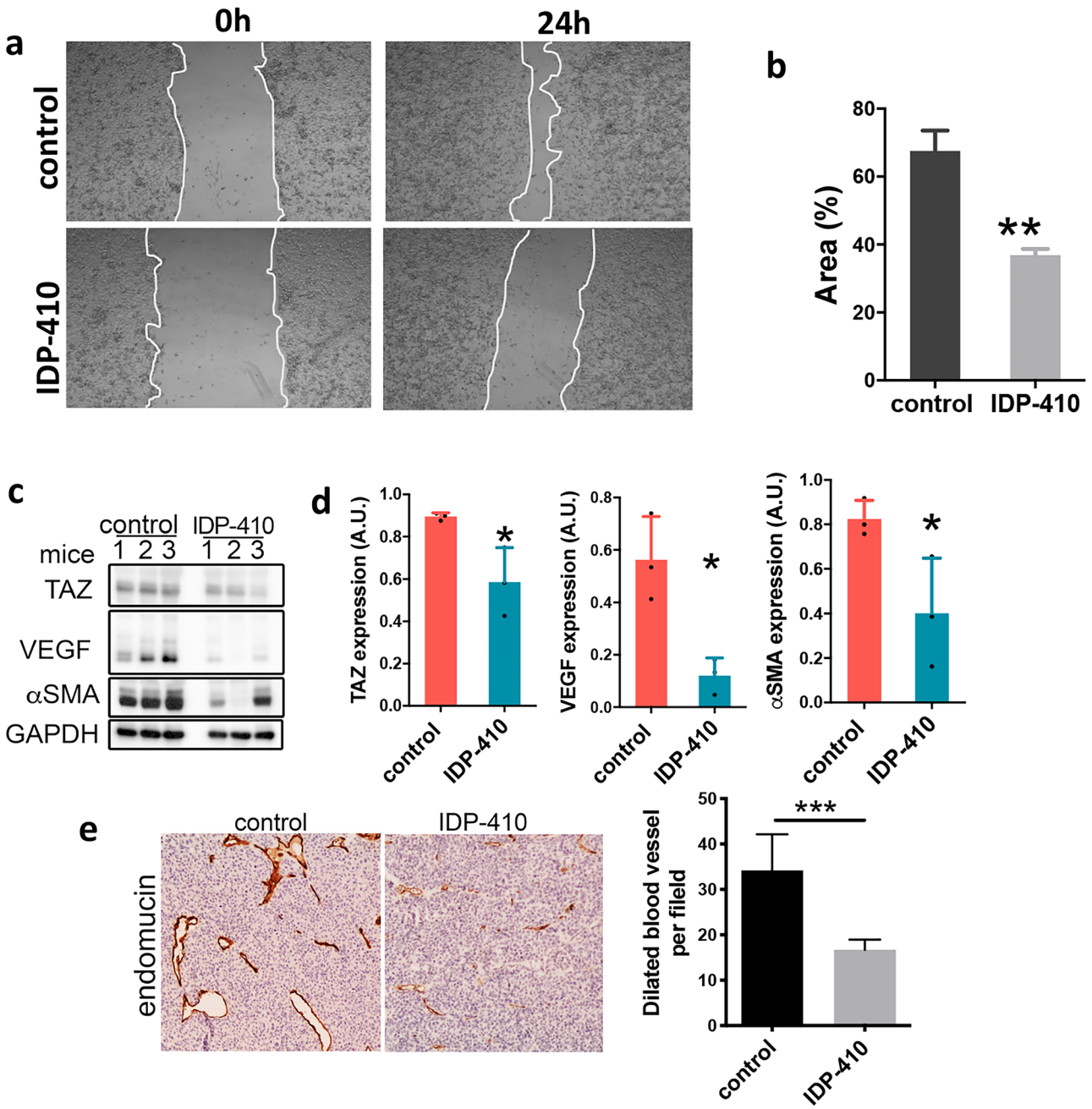

Fig. 7 IDP-410 impairs vascularization of gliomas. **a** Representative images from a wound healing test of HBMEC cells incubated in the presence of conditioned media from control or IDP-410 treated GBM6 cells. **b** Quantification of the percentage of the scratch area reduction in (**a**) (n = 4 / condition). **c–d** Western blot analysis of TAZ, VEGF, and αSMA in GBM6 tumors treated with vehicle (control) and IDP-410. GAPDH was used as a loading control. Quantification is shown in (**d**). **e** Representative pictures of the immunohistochemical staining of endomucin in GBM6 control and IDP-410 tumors. Quantification of the number of dilated blood vessels is shown on the right ($n = 3$) (n = 3 / condition). $^{**}p < 0.01$; $^{***}p < 0.001$

[46]. Our recent results indicate that these processes are mediated by increases in TAZ and α-SMA expression in glioma cells [29, 47]. TAZ controls the mesenchymal transformation of gliomas, which is associated with changes in the tumor milieu [36]. In addition, it has been shown that TAZ activation and stabilization could be induced by the hypoxic and pro-angiogenic tumor microenvironment in different cancers [48]. Moreover, this transcription factor works as a crucial VEGF-VEGFR2 signal transducer during developmental angiogenesis [49] and endothelial TAZ activation is needed for the formation of blood and lymphatic vessels [48]. These results suggest the existence of a

pro-angiogenic and mesenchymal feedback loop in normal and tumorigenic tissues. The expression analysis in gliomas treated with IDP-410 suggest a reduction in the expression of angiogenic factors, such as VEGFA. This could then led to the reduction of TAZ stability, decreasing the mesenchymal features of gliomas and further inhibiting the process of neo-vascularization. Altogether, these effects could be responsible for the reduced growth and aggressiveness of gliomas observed after N-MYC inhibition.

Overall, our data highlights the relevance of N-MYC in glioma pathology, and in particular its role via the stabilization of the protein. Moreover, we have demonstrated the efficacy and mechanism of action of IDP-410, a newly designed peptide that targets directly N-MYC protein. The results obtained shed some hope for a possible GBM stratified treatment, although further development, such as testing new formulations or delivery systems, is warranted to increase the anti-glioma effect of N-MYC inhibition. In addition, more insights into IDP-410's effects, and possible mechanisms of resistance need to be gathered. Especially interesting would be to study the effect of IDP-410 in the immune component of the microenvironment, and its combination with immune checkpoint inhibitors in GBM tumors, as MYC inhibitors can enhance the anti-tumoral immune response [50]. Moreover, combinatorial approaches with anti-angiogenic molecules, which have failed to block GBM growth [51], would be desirable. In any case, the results presented here shows the therapeutic potential of IDP-410 in GBM, as it disrupts the tumor microenvironment, which is a crucial regulator of tumor initiation and malignant progression, but is also involved in therapeutic resistance [52]. Targeting both the tumor cells and their supportive niche will probably be more efficient and will render the tumors less susceptible to the appearance of resistant subclones with different genetic alterations.

Supplementary Information The online version contains supplementary material available at https://doi.org/10.1007/s13311-021-01176-6.

Required Author Forms Disclosure forms provided by the authors are available with the online version of this article.

Funding This work was supported by Ministerio de Economía y Competitividad: (Acción Estratégica en Salud) and FEDER funds: PI16/01550 to JMS, by "Asociación Española contra el Cancer" grants: INVES192GARG to RG, GCTRA16015SEDA to JMS, and IDEAS-20095SÁNC to PSG, and by Ministerio de Ciencia, Innovación y Universidades and FEDER funds: RTI2018-093596 to PSG. MGA was supported by the Young Employment Initiative (Comunidad de Madrid).

Declarations

Competing Interests Laura Nevola and Santiago Esteban are co-founders and shareholders at IDP Discovery Pharma. This work was supported in part by IDP Discovery Pharma funds.

References

1. Louis DN, Wesseling P, Aldape K, Brat DJ, Capper D, Cree IA, et al. cIMPACT-NOW update 6: new entity and diagnostic principle recommendations of the cIMPACT-Utrecht meeting on future CNS tumor classification and grading. Brain Pathol. 2020.
2. Nieder C, Adam M, Molls M, Grosu AL. Therapeutic options for recurrent high-grade glioma in adult patients: recent advances. Crit Rev Oncol Hematol. 2006;60(3):181–93. https://doi.org/10.1016/j.critrevonc.2006.06.007.
3. Stupp R, Mason WP, van den Bent MJ, Weller M, Fisher B, Taphoorn MJ, et al. Radiotherapy plus concomitant and adjuvant temozolomide for glioblastoma. N Engl J Med. 2005;352(10):987–96. https://doi.org/10.1056/NEJMoa043330.
4. Wong ML, Kaye AH, Hovens CM. Targeting malignant glioma survival signalling to improve clinical outcomes. J Clin Neurosci. 2007;14(4):301–8. https://doi.org/10.1016/j.jocn.2006.11.005.
5. Chen A, Koehler AN. Transcription factor inhibition: lessons learned and emerging targets. Trends Mol Med. 2020;26(5):508–18. https://doi.org/10.1016/j.molmed.2020.01.004.
6. Albihn A, Johnsen JI, Henriksson MA. MYC in oncogenesis and as a target for cancer therapies. Adv Cancer Res. 2010;107:163–224. https://doi.org/10.1016/s0065-230x(10)07006-5.
7. Carroll PA, Freie BW, Mathsyaraja H, Eisenman RN. The MYC transcription factor network: balancing metabolism, proliferation and oncogenesis. Front Med. 2018;12(4):412–25. https://doi.org/10.1007/s11684-018-0650-z.
8. Lourenco C, Resetca D, Redel C, Lin P, MacDonald AS, Ciaccio R, et al. MYC protein interactors in gene transcription and cancer. Nat Rev Cancer. 2021;21(9):579–91.
9. Malynn BA, de Alboran IM, O'Hagan RC, Bronson R, Davidson L, DePinho RA, et al. N-myc can functionally replace c-myc in murine development, cellular growth, and differentiation. Genes Dev. 2000;14(11):1390–9.
10. Westermann F, Muth D, Benner A, Bauer T, Henrich K-O, Oberthuer A, et al. Distinct transcriptional MYCN/c-MYC activities are associated with spontaneous regression or malignant progression in neuroblastomas. Genome Biol. 2008;9(10):R150. https://doi.org/10.1186/gb-2008-9-10-r150.
11. Northcott PA, Shih DJ, Peacock J, Garzia L, Morrissy AS, Zichner T, et al. Subgroup-specific structural variation across 1,000 medulloblastoma genomes. Nature. 2012;488(7409):49–56. https://doi.org/10.1038/nature11327.
12. Bretones G, Delgado MD, León J. Myc and cell cycle control. Biochim Biophys Acta. 2015;1849(5):506–16. https://doi.org/10.1016/j.bbagrm.2014.03.013.
13. Borgenvik A, Cancer M, Hutter S, Swartling FJ. Targeting MYCN in molecularly defined malignant brain tumors. Front Oncol. 2020;10:626751. https://doi.org/10.3389/fonc.2020.626751.
14. Swartling FJ, Savov V, Persson AI, Chen J, Hackett CS, Northcott PA, et al. Distinct neural stem cell populations give rise to disparate brain tumors in response to N-MYC. Cancer Cell. 2012;21(5):601–13. https://doi.org/10.1016/j.ccr.2012.04.012.
15. Faria MH, Khayat AS, Burbano RR, Rabenhorst SH. c-MYC amplification and expression in astrocytic tumors. Acta Neuropathol. 2008;116(1):87–95. https://doi.org/10.1007/s00401-008-0368-0.
16. Orian JM, Vasilopoulos K, Yoshida S, Kaye AH, Chow CW, Gonzales MF. Overexpression of multiple oncogenes related to histological grade of astrocytic glioma. Br J Cancer. 1992;66(1):106–12. https://doi.org/10.1038/bjc.1992.225.
17. Herms JW, von Loewenich FD, Behnke J, Markakis E, Kretzschmar HA. c-myc oncogene family expression in glioblastoma and survival. Surg Neurol. 1999;51(5):536–42. https://doi.org/10.1016/s0090-3019(98)00028-7.

18. Hui AB, Lo KW, Yin XL, Poon WS, Ng HK. Detection of multiple gene amplifications in glioblastoma multiforme using array-based comparative genomic hybridization. Lab Invest. 2001;81(5):717–23. https://doi.org/10.1038/labinvest.3780280.
19. Hodgson JG, Yeh RF, Ray A, Wang NJ, Smirnov I, Yu M, et al. Comparative analyses of gene copy number and mRNA expression in glioblastoma multiforme tumors and xenografts. Neuro Oncol. 2009;11(5):477–87. https://doi.org/10.1215/15228517-2008-113.
20. Zheng H, Ying H, Yan H, Kimmelman AC, Hiller DJ, Chen AJ, et al. p53 and Pten control neural and glioma stem/progenitor cell renewal and differentiation. Nature. 2008;455(7216):1129–33. https://doi.org/10.1038/nature07443.
21. Fukasawa K, Kadota T, Horie T, Tokumura K, Terada R, Kitaguchi Y, et al. CDK8 maintains stemness and tumorigenicity of glioma stem cells by regulating the c-MYC pathway. Oncogene. 2021;40(15):2803–15. https://doi.org/10.1038/s41388-021-01745-1.
22. Fuertes G, Nevola L, Esteban-Martín S. Chapter 9 - Perspectives on drug discovery strategies based on IDPs. In: Salvi N, editor. Intrinsically disordered proteins. Academic Press; 2019. p. 275–327.
23. McAnulty J, DiFeo A. The molecular 'Myc-anisms' behind Myc-driven tumorigenesis and the relevant Myc-directed therapeutics. Int J Mol Sci. 2020. https://doi.org/10.3390/ijms21249486.
24. Liu Z, Chen SS, Clarke S, Veschi V, Thiele CJ. Targeting MYCN in pediatric and adult cancers. Front Oncol. 2020;10:623679. https://doi.org/10.3389/fonc.2020.623679.
25. Wang C, Zhang J, Yin J, Gan Y, Xu S, Gu Y, et al. Alternative approaches to target Myc for cancer treatment. Signal Transduct Target Ther. 2021;6(1):117. https://doi.org/10.1038/s41392-021-00500-y.
26. Whitfield JR, Beaulieu ME, Soucek L. Strategies to inhibit Myc and their clinical applicability. Front Cell Dev Biol. 2017;5:10. https://doi.org/10.3389/fcell.2017.00010.
27. Bayliss R, Burgess SG, Leen E, Richards MW. A moving target: structure and disorder in pursuit of Myc inhibitors. Biochem Soc Trans. 2017;45(3):709–17. https://doi.org/10.1042/bst20160328.
28. Pozo N, Zahonero C, Fernandez P, Linares JM, Ayuso A, Hagiwara M, et al. Inhibition of DYRK1A destabilizes EGFR and reduces EGFR-dependent glioblastoma growth. J Clin Investig. 2013;123(6):2475–87. https://doi.org/10.1172/JCI63623.
29. Gargini R, Segura-Collar B, Herranz B, Garcia-Escudero V, Romero-Bravo A, Nunez FJ, et al. The IDH-TAU-EGFR triad defines the neovascular landscape of diffuse gliomas. Sci Transl Med. 2020;12(527).
30. Miller SJ, Blackwell HE, Grubbs RH. Application of ring-closing metathesis to the synthesis of rigidified amino acids and peptides. J Am Chem Soc. 1996;118(40):9606–14. https://doi.org/10.1021/ja961626l.
31. Hardee ME, Zagzag D. Mechanisms of glioma-associated neovascularization. AmJPathol. 2012;181(4):1126–41.
32. Meškytė EM, Keskas S, Ciribilli Y. MYC as a multifaceted regulator of tumor microenvironment leading to metastasis. Int J Mol Sci. 2020. https://doi.org/10.3390/ijms21207710.
33. Chanthery YH, Gustafson WC, Itsara M, Persson A, Hackett CS, Grimmer M, et al. Paracrine signaling through MYCN enhances tumor-vascular interactions in neuroblastoma. Sci Transl Med. 2012;4(115):115ra3. https://doi.org/10.1126/scitranslmed.3002977.
34. Ma L, Young J, Prabhala H, Pan E, Mestdagh P, Muth D, et al. miR-9, a MYC/MYCN-activated microRNA, regulates E-cadherin and cancer metastasis. Nat Cell Biol. 2010;12(3):247–56. https://doi.org/10.1038/ncb2024.
35. Sharma S, Goswami R, Zhang DX, Rahaman SO. TRPV4 regulates matrix stiffness and TGFβ1-induced epithelial-mesenchymal transition. J Cell Mol Med. 2019;23(2):761–74. https://doi.org/10.1111/jcmm.13972.
36. Bhat KP, Salazar KL, Balasubramaniyan V, Wani K, Heathcock L, Hollingsworth F, et al. The transcriptional coactivator TAZ regulates mesenchymal differentiation in malignant glioma. Genes Dev. 2011;25(24):2594–609.
37. Gargini R, Segura-Collar B, Sánchez-Gómez P. Cellular plasticity and tumor microenvironment in gliomas: the struggle to hit a moving target. Cancers (Basel). 2020. https://doi.org/10.3390/cancers12061622.
38. Soucek L, Whitfield J, Martins CP, Finch AJ, Murphy DJ, Sodir NM, et al. Modelling Myc inhibition as a cancer therapy. Nature. 2008;455(7213):679–83. https://doi.org/10.1038/nature07260.
39. Beaulieu ME, Jauset T, Massó-Vallés D, Martínez-Martín S, Rahl P, Maltais L, et al. Intrinsic cell-penetrating activity propels Omomyc from proof of concept to viable anti-MYC therapy. Sci Transl Med. 2019. https://doi.org/10.1126/scitranslmed.aar5012.
40. Annibali D, Whitfield JR, Favuzzi E, Jauset T, Serrano E, Cuartas I, et al. Myc inhibition is effective against glioma and reveals a role for Myc in proficient mitosis. Nat Commun. 2014;5(1):4632. https://doi.org/10.1038/ncomms5632.
41. Gerhardt H, Golding M, Fruttiger M, Ruhrberg C, Lundkvist A, Abramsson A, et al. VEGF guides angiogenic sprouting utilizing endothelial tip cell filopodia. J Cell Biol. 2003;161(6):1163–77. https://doi.org/10.1083/jcb.200302047.
42. Akeson A, Herman A, Wiginton D, Greenberg J. Endothelial cell activation in a VEGF-A gradient: relevance to cell fate decisions. Microvasc Res. 2010;80(1):65–74. https://doi.org/10.1016/j.mvr.2010.02.001.
43. Bautch VL. VEGF-directed blood vessel patterning: from cells to organism. Cold Spring Harb Perspect Med. 2012;2(9):a006452. https://doi.org/10.1101/cshperspect.a006452.
44. Whitfield JR, Soucek L. Tumor microenvironment: becoming sick of Myc. Cell Mol Life Sci. 2012;69(6):931–4. https://doi.org/10.1007/s00018-011-0860-x.
45. Meitar D, Crawford SE, Rademaker AW, Cohn SL. Tumor angiogenesis correlates with metastatic disease, N-myc amplification, and poor outcome in human neuroblastoma. J Clin Oncol. 1996;14(2):405–14. https://doi.org/10.1200/jco.1996.14.2.405.
46. Cheng L, Huang Z, Zhou W, Wu Q, Donnola S, Liu JK, et al. Glioblastoma stem cells generate vascular pericytes to support vessel function and tumor growth. Cell. 2013;153(1):139–52.
47. Segura-Collar B, Garranzo-Asensio M, Herranz B, Hernández-SanMiguel E, Cejalvo T, Casas BS, et al. Tumor-derived pericytes driven by EGFR mutations govern the vascular and immune microenvironment of gliomas. Cancer Res. 2021. https://doi.org/10.1158/0008-5472.can-20-3558.
48. Hooglugt A, van der Stoel MM, Boon RA, Huveneers S. Endothelial YAP/TAZ signaling in angiogenesis and tumor vasculature. Front Oncol. 2020;10:612802. https://doi.org/10.3389/fonc.2020.612802.
49. Wang X, Freire Valls A, Schermann G, Shen Y, Moya IM, Castro L, et al. YAP/TAZ Orchestrate VEGF signaling during developmental angiogenesis. Dev Cell. 2017;42(5):462-78.e7. https://doi.org/10.1016/j.devcel.2017.08.002.
50. Han H, Jain AD, Truica MI, Izquierdo-Ferrer J, Anker JF, Lysy B, et al. Small-molecule MYC inhibitors suppress tumor growth and enhance immunotherapy. Cancer Cell. 2019;36(5):483-97.e15. https://doi.org/10.1016/j.ccell.2019.10.001.
51. Wang N, Jain RK, Batchelor TT. New directions in anti-angiogenic therapy for glioblastoma. Neurotherapeutics. 2017;14(2):321–32. https://doi.org/10.1007/s13311-016-0510-y.
52. Wu P, Gao W, Su M, Nice EC, Zhang W, Lin J, et al. Adaptive Mechanisms of tumor therapy resistance driven by tumor microenvironment. Front Cell Dev Biol. 2021;9:357.